Power Outage and Environmental Justice in Winter Storm Uri: An Analytical Workflow Based on Nighttime Light Remote Sensing

Abstract

With the increasing intensity of extreme weather events, human society faces an unprecedented threat of personal injuries, fatalities, and economic losses. As a major component in lifeline infrastructures, electrical power system is of significance to human communities. In severe weather events, it is important to identify impact areas of power outages and affected communities, and thus provide support for informed decision-making for disaster response and relief. However, the lack of household-level power outage data creates challenges for timely and precise power outage assessments. To address these challenges, we introduced an analytical workflow that applies NASA's Black Marble daily nighttime light (NTL) images to detect power outages in the 2021 Winter Storm Uri. This workflow includes adjustment processes to reduce the effects of viewing angle and snow reflection. Power outage is detected by comparing NTL images in the storm and NTL images in a normal condition (baseline) using an empirical adjusted equation. Outcomes of the workflow are 500-meter resolution power outage maps, which were found to have the highest consistency with real outage tracking data when NTL intensity was reduced by 26%. With the resultant power outage maps, we analyzed the relations between power outages and ratios of disadvantaged populations in 126 Texas counties and 4182 census tracts to evaluate environmental justice in the storm. The results show that Latino/Hispanic communities tend to suffer more from power outages at both the county and census tract levels.

Keywords: nighttime light, disaster resilience, natural disaster, spatial analysis, environmental justice, power outage

Highlights

- Introduced an analytical workflow to detect power outages from NASA's daily Black Marble nighttime light (NTL) remote sensing images.
- Developed radiance adjustment algorithms to mitigate the effects of viewing angle and snow cover to NTL radiance
- Analyzed environmental justice issues related to power outages in 2021 Winter Storm Uri
- Latino/Hispanic communities tend to be more impacted by power outages in the storm

1. Introduction

With the changing climate, an increasing number and intensity of extreme weather events, such as hurricanes, winter storms, thunderstorms, and tornadoes, pose an unprecedented threat to human society. The serviceability of critical infrastructures (CIs) during extreme weather events is of critical importance to socio-economic activities (Deshmukh et al., 2011). Published evidence shows that disinvestment and poor maintenance of CIs often lead to greater losses in human communities (Chang, 2003; Mastroianni et al., 2021). Additionally, disruptions of CIs in extreme weather events may add extra burdens to disadvantaged communities (Hendricks & Van Zandt, 2021). Thus, the serviceability and resilience of CIs in extreme events are often associated with social equality and environmental justice. As lifeline infrastructure systems, electrical power systems are critical for socioeconomic activities but vulnerable to multiple types of hazards. The failures of electric power systems may trigger a series of cascading effects (Kwasinski et al., 2019). Long-lasting blackouts affect food and water supplies, disrupting communication and leaving people in discomforting conditions (e.g., heat, cold, and darkness) (Casey et al., 2020; Klinger et al., 2014). When combined with freezing temperatures, blackouts can cause damage to building structures and pose threats to people's lives and health (Dominianni et al., 2018). Underserved and marginalized population groups often suffer greater impacts due to the lack of adaptive capacities (Min et al., 2017). Thus, timely and fine-resolution assessments of power outages in extreme weather events are of critical importance for emergency response, disaster relief, and policymaking to mitigate inequalities and injustice in disasters.

However, monitoring power outages in extreme weather events faces challenges. First, household-level power outage data are not publicly available due to privacy concerns (Boroojeni

et al., 2017). According to reports from the U.S. Energy Information Administration (EIA) (Alexander & Sara, 2017; Tweed, 2016), only a small proportion of the population agrees to share data about electricity consumption and outage with a third party, let alone the public. To protect individuals' privacy, power outage data are usually aggregated at coarse spatial units (e.g., cities and counties), which are not sufficient to guide emergency response and resilience assessment at the neighborhood level. Second, multiple electric providers serving the same area create challenges to acquire complete outage data. For example, Texas is served by more than 100 electric utility companies, some of which have overlapped serving areas (Public Utility Commission of Texas, 2022). Due to different tracking standards and methods, different utility companies may provide inconsistent power outage data. Additionally, the total number of blackouts in a disaster, which synthesizes household surveys or outage tracking devices, can take a long time to conclude (Cole et al., 2017), impeding timely actions for disaster response and relief. The data collected from surveys and power tracking devices only cover a small population sample and may overlook certain disadvantaged population groups. To overcome these issues, alternative data sources have been explored to detect power outages. For instance, Volunteered Geographic Information (VGI) (e.g., social media) can provide a considerable amount of data on the population impacted by power outages (Goodchild, 2007; Guan & Chen, 2014; L. Li et al., 2020; Mao et al., 2018). A few studies have detected spatial and temporal distributions of power outages by mining social media data (Mao et al., 2018; Sun et al., 2016), despite the concerns of biased user demography and data uncertainty (Ribeiro et al., 2018, 2020). Thus, there is a pressing need to leverage alternative data sources to develop timely and reliable power outage assessments to support disaster response and resilience enhancement.

With the ability to detect artificial lights on the earth's surface, nighttime light (NTL) remote sensing radiometers are a promising instrument to assess disaster impacts on human communities and CIs. In previous studies, NTL images are primarily used to assess disaster impact and damage (Xu & Qiang, 2021; Zhao et al., 2018) and monitor the recovery of human activities (Qiang et al., 2020). Pioneer work has been conducted to detect power outages from time series of NTL images. For example, Wang et al. (2018) introduced the use of NTL radiance from NASA's Black Marble images to detect the spatial extent of outages during Hurricane Sandy in 2012 and Hurricane Maria in 2017. A few studies (e.g., Román et al. (2019) and Azad & Ghandehari (2021)) used the Black Marble images to monitor electricity restoration during Hurricane Maria and discovered social and geographic disparities in electric restoration among Puerto Rican communities. A major issue in the previous studies is the lack of empirical validation, which raises doubts about the accuracy of power outage detection. Additionally, the previous studies simply used original NTL radiance in the remote sensing images to detect power outages, without addressing biases introduced by extraneous factors, such as the viewing angle and snow reflection (Wang et al., 2021). These uncertainties can be amplified by the changing atmospheric and ground conditions in extreme weather events, which can further affect the validity of outage detection results.

In this study, we introduced an analytical workflow that applies NASA's Black Marble nighttime light (NTL) daily images to detect power outages in 2021 Winter Storm Uri (Fig. 1). This workflow includes radiance adjustments to reduce the effects of viewing angle and snow reflection on the NTL radiance. Additionally, novel approaches were introduced to determine the baseline radiance (radiance captured in the normal condition) and the radiance reduction threshold for power outage detection. The workflow generated power outage maps at a 15-arc-

second resolution (approximately 500 meters) covering the entire declared disaster areas, enabling various analyses from the neighborhood scale to the county or city scale. Finally, we overlaid the power outage maps with socio-economic variables to evaluate environmental justice in the storm. Our hypothesis is that disadvantaged populations are disproportionally exposed to power outages and correlation analysis was used to test the hypothesis. The developed workflow can be used as an actionable tool to produce timely and scaled power outage detection from publicly available data. Meanwhile, the analysis will provide important information for developing sustainable, resilient, and equitable communities in the face of increasing extreme weather events in the changing climate.

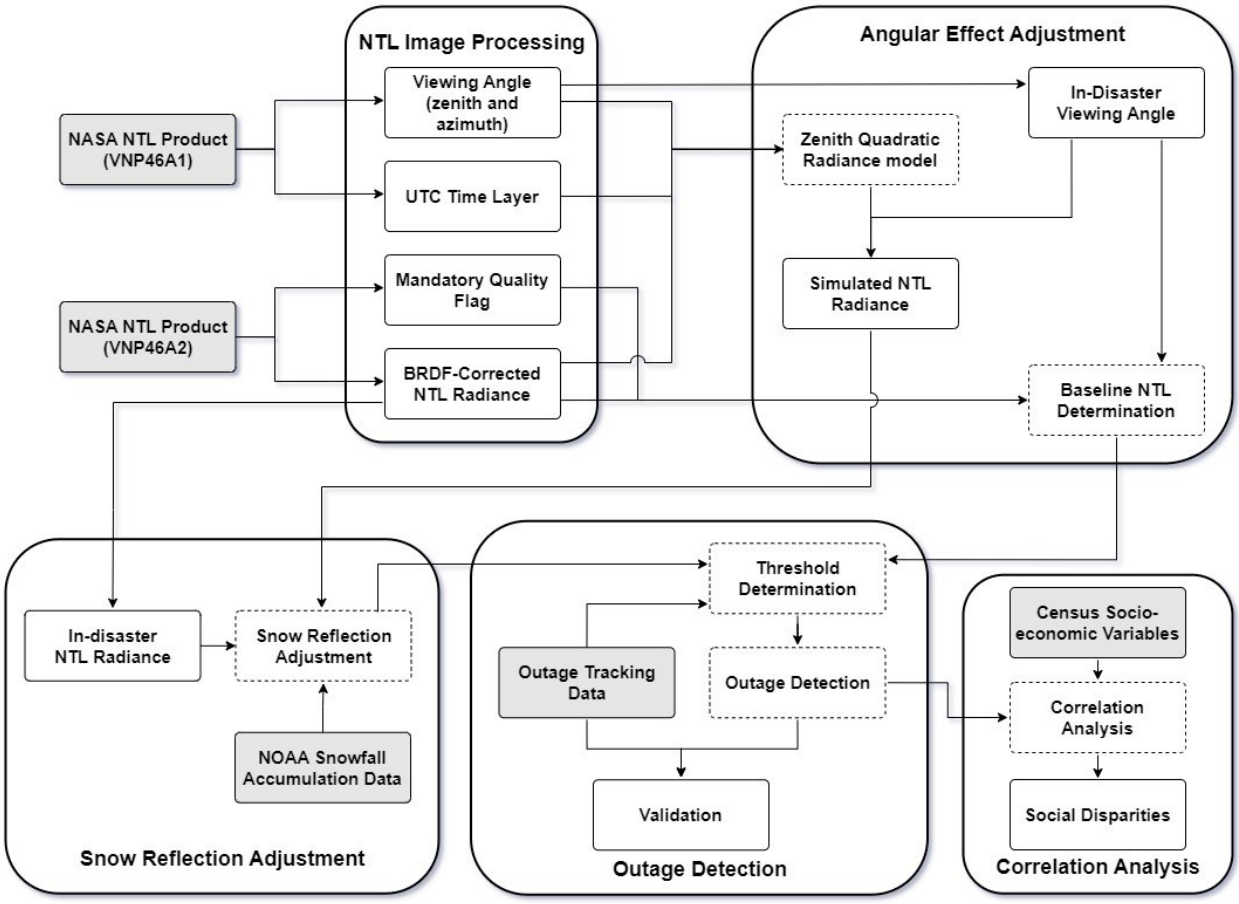

Fig. 1. Workflow of outage detection using NASA's Black Marble product suites

2. Datasets

2.1 Study Area

Winter Storm Uri, also named Valentine's week winter outbreak 2021 by National Oceanic and Atmospheric Administration (NOAA), emerged on Feb 11th, and dissipated on Feb 20th. Due to this storm, a winter storm warning has been issued for the entire state of Texas and multiple states in the U.S. Midwest and Southern Plains (Fig. 2(a)). As one of the most affected states, Texas was hit by massive snow, sleet, freezing rain, and low temperature. The storm resulted in a death toll of 246 people and an economic loss of over 195 billion dollars, which makes Uri the costliest winter storm on record (Ivanova, 2021). As a critical infrastructure, the electric power system in Texas was seriously disrupted and caused extensive blackouts lasting for several days (Lee et al., 2021). The Texas Interconnection network, the largest electric grid in Texas, generated rolling blackouts across the whole state of Texas, which affected 4 million people (Rice & Aspegren, 2021). Due to Uri's devastating impacts, President Joseph R. Biden approved three major disaster declaration orders for a total of 126 Texas counties (Federal Agency Management Agency, 2021a, 2021c, 2021b). As Texas has a large area of undeveloped lands where NTL emissions may not be generated from human activities, the result of NTL radiance adjustment on all pixels within Texas can be biased towards the large numbers of non-urban pixels with minimal NTL radiance. Besides, surface oil wells outside urban areas can generate high NTL radiance, but these locations do not represent populations affected by power outages. To eliminate such conspicuous brightness in rural areas, our study focuses on urban areas where the impervious surface area (ISA) ratio is above 0.5. The ISA ratio is the ratio of impervious surface pixels to the total pixels in the LULC data, which is calculated within each pixel in the NTL image.

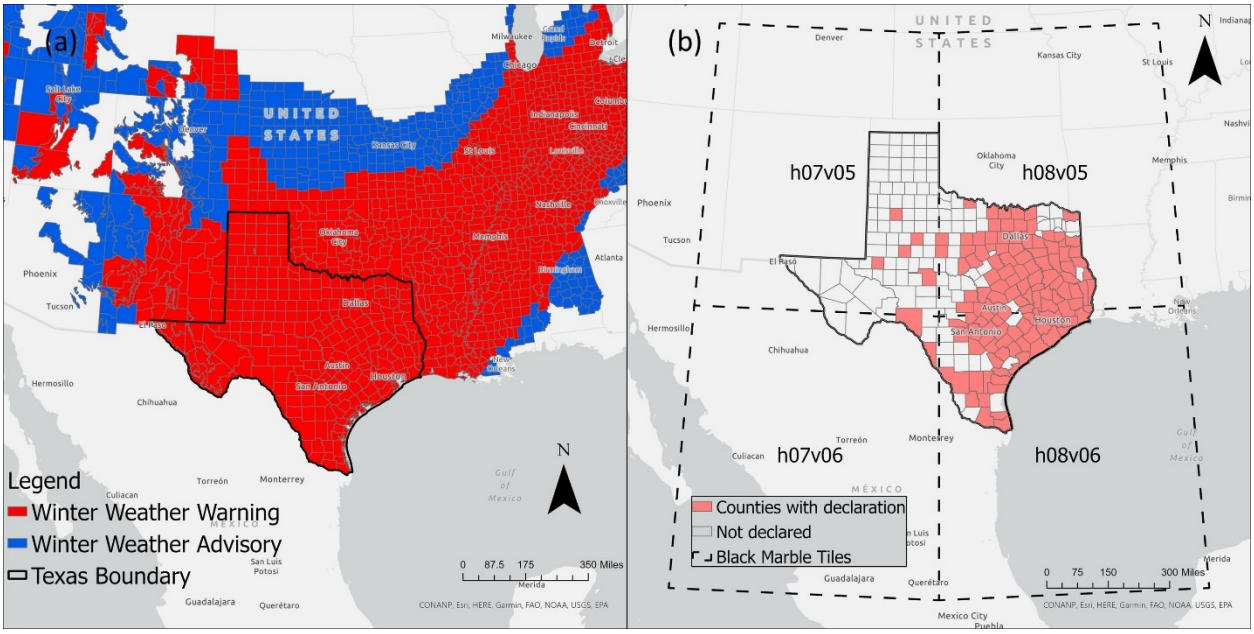

Fig. 2. a) National Weather Services (NWS) winter weather forecast near Texas, b) counties that declared Winter Storm Uri as a major disaster

2.2 Data

2.2.1 Nighttime Light Images

NASA's Black Marble daily images (VNP46) were utilized to detect power outages. Black Marble images were collected from the Visible Infrared Imaging Radiometer Suite (VIIRS) day/night band (DNB) sensor of the Suomi National Polar-Orbiting Partnership (SNPP) satellite. The Black Marble product suite includes two products: VNP46A1 and VNP46A2. VNP46A1 offers a consistent temporal scale at the daily level with a spatial resolution at 15-arc-second (around 500 meters in the study area) and overcomes the saturation effect and onboard calibration issue in the preceding NTL product. The VNP46A2 product includes 6 layers that were processed from the VNP46A1 product by removing biases from irrelevant NTL sources

(e.g., moonlight, atmospheric effect) using the bidirectional reflectance distribution function (BRDF) model inversion (Román et al., 2018; Román, Wang, et al., 2019). In this study, the NTL radiance (DNB_BRDF-Corrected_NTL layer) in the VNP46A2 product was used to detect blackouts in Texas during the winter storm. Meanwhile, the viewing zenith and azimuth angles in VNP46A1 were used to adjust the angular effect. Images from Jan 1, 2020, to Mar 2, 2021, were downloaded from the Level-1 and Atmosphere Archive & Distribution System (LAADS) Distributed Active Archive Center (DAAC) Portal (https://ladsweb.modaps.eosdis.nasa.gov/search/). Fig. 2(b) shows the four tiles (dashed line) of Black Marble images used in this study, which were mosaicked to cover the whole study area. The parameters of layers extracted from Black Marble products are summarized in Table 1.

Table 1. Descriptions of layers extracted from NASA's Black Marble product

Layer	Value Range	Product
Sensor Viewing Zenith	Ranging from -90° to 90°	VNP46A1
Sensor Viewing Azimuth	Ranging from -180° to 180°, 0° represents the north direction, negative values represent the east, and positive values represent the west	VNP46A1
UTC Time	Ranging from -12 to 12, represent time in the UTC	VNP46A1
BRDF-corrected Radiance	Ranging from 0 to 6553.4	VNP46A2
Mandatory Quality Flag (QF)	00 (high-quality & persistent), 01 (high-quality & ephemeral), 02 (poor-quality), 255 (no retrieval)	VNP46A2

2.2.2 Auxiliary Data

In addition to the NTL images, several auxiliary datasets were used in this study. First, hourly power outage data at the county level from Feb 10, 2021 to Feb 25, 2021 were purchased from BlueFire Studios LLC (http://poweroutage.us) to calculate the power outage detection model. This dataset summarized power outage tracking data from 61 electricity providers during Uri in Texas. Second, the most recent land use and land cover data (LULC) from the National Land

Cover Database 2019 (NLCD 2019) were used to calculate the impervious surface area (ISA) ratios in NTL image pixels (Dewitz & U.S. Geological Survey, 2021; Homer et al., 2020; Jin et al., 2019; Wickham et al., 2021; Yang et al., 2018). Pixels with a ratio of ISA > 0.5 were considered urban areas and selected as the study area. Third, socio-economic variables at the census-tract and county level were acquired from the 2019 American Community Survey (Table 2). These socio-economic variables are common indicators in community resilience assessment (Cutter et al., 2003; Lam et al., 2016) and are available in the American Community Survey data. These variables were used to analyze the relations between the detected power outages and socio-economic conditions of communities. Fourth, snow accumulation data were collected from NOAA National Gridded Snowfall Analysis (https://www.nohrsc.noaa.gov/snowfall/). Due to the heavy cloud cover during and after the winter storm, snow accumulation data from NOAA is the only data source that covers the whole research area and has a fine temporal granularity (updated every 12 hours).

Table 2. The list of tables and socio-economic variables extracted from the 2019 American Community Survey

Variable Name	**Description**
Ratio of White	Ratio of White American population (one race) to total population
Ratio of African American	Ratio of African American population (one race) to total population
Ratio of American Indian and Alaska Native	Ratio of American Indian and Alaska Native population (one race) to total population
Ratio of Asian	Ratio of Asian American (one race) to total population
Ratio of Latino/Hispanic	Ratio of Latino/Hispanic population to total population
Ratio of 25 years old + and hold a degree less than college degree	Ratio of population over 25 years old and with a degree lower than a college degree to total population
Ratio of commute time less than 30 minutes	Ratio of population living in areas with less than 30 minutes commuting time
Ratio of income lower than poverty level	Ratio of population with income lower than the poverty level to total population
Median household income	Median household income in the past 12 months (in 2019 inflation-adjusted dollars)

Variable Name	Description
Unemployment ratio	Ratio of unemployed population to total population in labor forces
Renter-occupied housing ratio	Ratio of renter-occupied housing units to total housing units
Ratio of constructions built after 2000	Ratio of constructions built before 2000 to total housing units
Median housing value	Median value of owner-occupied housing units in dollars
Median gross rent	Median gross rent of renter-occupied housing units paying cash rent

2.2.3 NTL Date Selection

Next, we determine the dates of NTL images for power outage detection. This selection is made with two criteria: (1) the images should be captured when extensive power outages occurred, and (2) the study area should have a clear sky (less cloud coverage). For the first criterion, the hourly ratio of power outages was calculated from the power outage tracking data from Bluefire Studios LLC. The ratio is the division of total outage hours by total tracked hours. The hourly outage ratio and its 24-hour moving average are displayed in Fig. 3, which shows that the extensive power outage lasted from Feb 15 to Feb 18 with a peak on Feb 16. For the second criterion, we calculated the number of counties that have > 80% high-quality NTL pixels (clear sky) each day, which is represented as gray bars in Fig. 3. Pixels in the VNP46A2 images where the value of the Mandatory Quality Flag (QF) is 00 are defined as high-quality pixels and selected for the analyses in this study. QF 01 pixels include ephemeral radiance, such as wildfire and lightning, which cannot represent a persistent human settlement. Also, QF 01 pixels are very few in the selected images (e.g., no QF 01 pixels on Feb 16). Thus, we decided to exclude QF 01 pixels in the analyses. Fig. 3 shows that the highest number of counties with a clear sky during the power outage period occurred on Feb 16, when 197 of the 254 counties have >80% coverage of high-quality pixels (QF 00). Thus, NTL images on Feb 16 meet both criteria and are selected to detect

power outages in the following analysis.

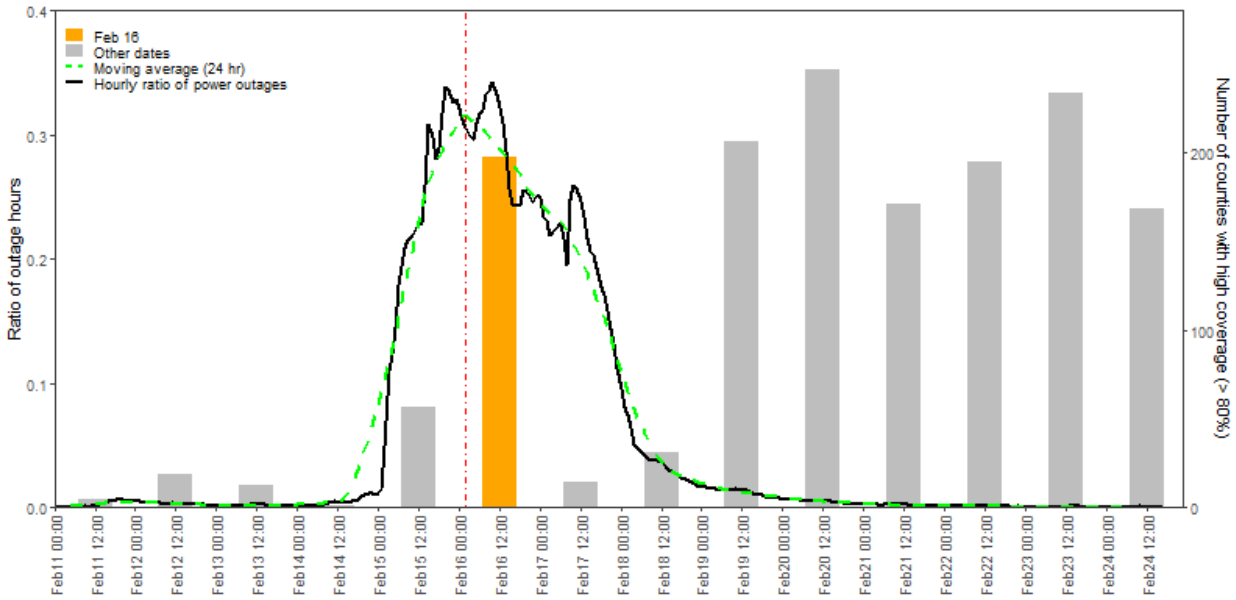

Fig. 3. Hourly ratio of power outage from Feb 11 to Feb 24 (lines, left axis) and the number of counties where > 80% area is covered by high-quality NTL pixels (bars, right axis). The red dashed line indicates the general NTL acquisition time (close to 2:45 am Central Standard Time) of NTL images on Feb 16, 2021

The NTL images on Feb 16 were captured between 2:45 AM to 2:50 AM in Central Standard Time (CST) as shown in Fig. 4(a). Thus, power outage tracking data between 2:00 AM and 3:00 AM on Feb 16 (highlighted in Fig. 3, red dashed lines) were selected to adjust the NTL radiance in the following steps. Fig. 4(b) shows the county-level outage ratios between 2-3 AM CST on Feb 16.

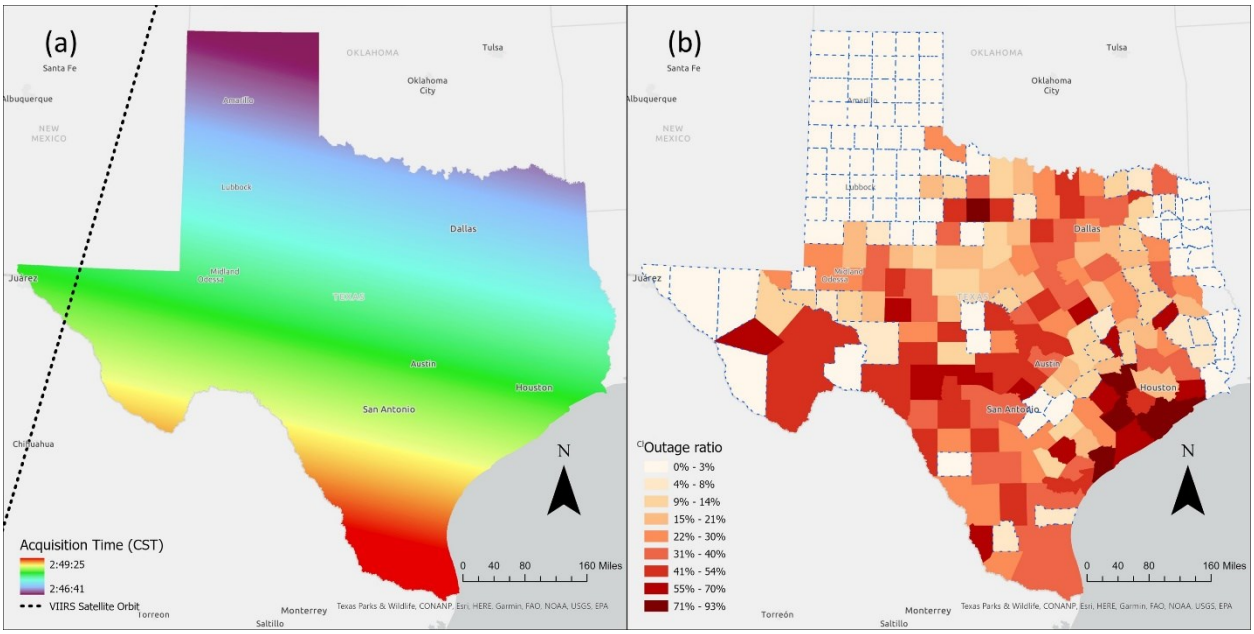

Fig. 4. (a) Acquisition time in Central Standard Time (CST) and VIIRS satellite orbit from VNP46A2 on Feb 16, 2021; (b) Power outage ratios (tracking data) between 2-3 AM in Texas counties, areas that did not experience extensive power outages are highlighted in blue dashed boundaries.

3. NTL Radiance Adjustment

Power outages can be detected by comparing the NTL radiance during outages and the radiance in the normal condition (baseline). However, the various viewing angles and snow reflection may affect the NTL radiance captured in the images and introduce biases to the comparison (Wang et al., 2021). Thus, a radiance adjustment is needed to eliminate the biases and make the images comparable. This section introduces the adjustment process that removes the angular effect and snow reflection in the NTL images.

3.1 Angular Effect

The viewing angle of the satellite sensor may affect the NTL radiance captured in images. Previous studies show that the relation between the viewing zenith angle and NTL radiance can be fitted into a quadratic equation (X. Li et al., 2019; Tan et al., 2022). This equation is known as the Zenith-Radiance Quadratic (ZRQ) model and can be expressed as Eq. 1:

$$R_{simulated} = a * VZA^2 + b * VZA + c \quad \text{Eq. 1}$$

where R stands for the nighttime light radiance, VZA means the viewing zenith angle, and a, b, and c are the coefficients.

The actual effects of the zenith angle may vary in the geographic space due to different land cover types and radiance levels. Fig. 5 shows the variation of zenith-radiance relations at four randomly selected pixels in the study area, where shapes of the quadratic fitting curve between NTL radiance and viewing zenith angle are different, meaning that the coefficients a, b, and c in Eq. 1 vary at different pixels. Thus, instead of using a global model to adjust the entire study area, we fit the ZRQ model locally at each pixel using NTL values from Jan 1, 2020, to Jan 31, 2021. To minimize the impact of the azimuth viewing angle, we selected data points on dates that have the same viewing direction (east or west) on Feb 16 to fit in the ZRQ model. According to the Interquartile Rule (Upton & Cook, 1996), NTL values that fall outside the +/− 1.5 interquartile range from the median value were considered outliers and excluded in the model fitting (red dots in Fig. 5). R programs are developed to automate this local fitting process. Using the locally-fitted ZRQ models, the expected NTL radiance in the viewing zenith angle on Feb 16 was simulated (orange dots in Fig. 5).

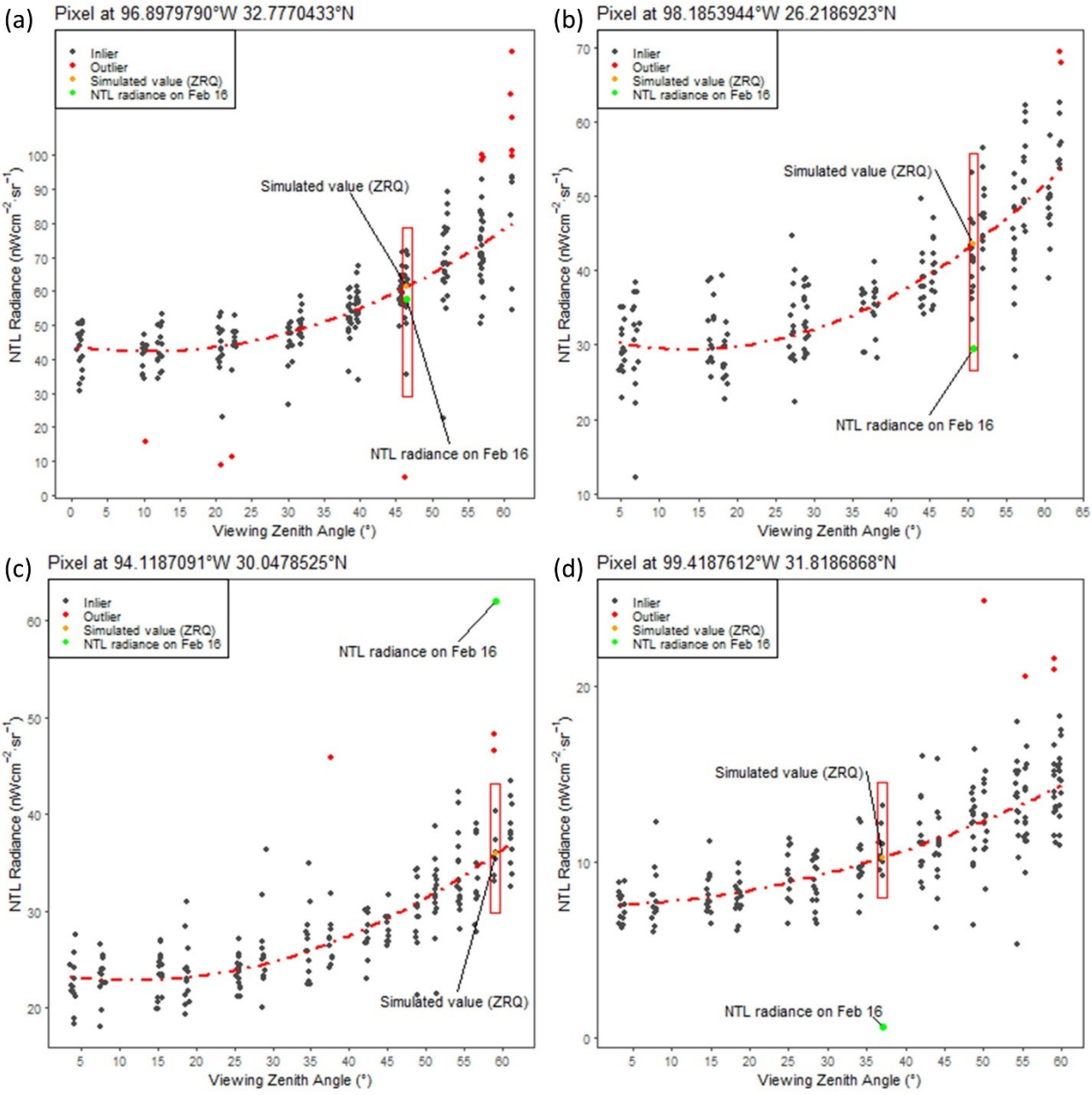

Fig. 5. Scatterplots of radiance by zenith angle from Jan 1, 2020, to Mar 2, 2021, in random four pixels in the study area. The red box indicates the radiance values on dates that have a similar viewing zenith angle as Feb 16, 2021

Fig. 6(a) shows the ratio of differences between the $R_{simulated}$ and R_{actual} at the pixel level (denoted as D), which is calculated using Eq. 2:

$$D = \frac{R_{actual} - R_{simulated}}{R_{simulated}} \quad \text{Eq. 2}$$

where R_{actual} is the actual radiance on Feb 16, and $R_{simulated}$ is the simulated NTL radiance on Feb 16, 2021, using the ZRQ model (Eq. 1).

The red pixels in Fig. 6(a) have a larger radiance value than the simulated (expected) value ($D > 0$) on Feb 16. Most of the red pixels are located at higher latitudes (north). These larger-than-expected radiance values contradict our expectation that power outages and reduced human activities would dim NTL radiance in the storm. This phenomenon is possibly due to the snow-covered land surface that can enhance NTL radiance (Levin & Zhang, 2017; Wang et al., 2021). Thus, we conducted the following analysis to evaluate the effect of snow reflection on the NTL radiance,

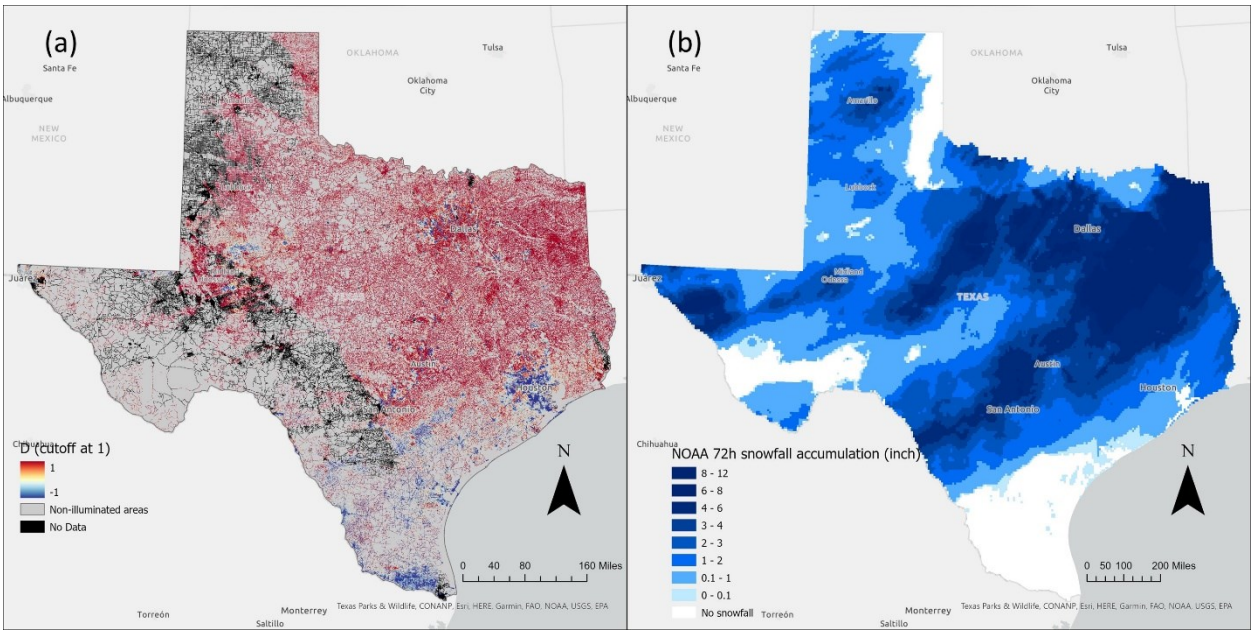

Fig. 6. Comparison between NTL radiance change and snow accumulation. (a) Spatial distribution of NTL radiance change (D). (b) NOAA National Gridded Snowfall Analysis (72-hour snowfall accumulation) at 12:00 AM, Feb 16, 2021

3.2 Snow Reflection

We developed an additional adjustment process to reduce the snow effect on NTL radiance. After evaluating multiple sources for snow data, including MODIS Snow Cover (MOD10), VIIRS/NPP Snow Cover (VNP10), and ground images from Sentinel-2 and Landsat-8, we found these products are heavily impacted by cloud coverage in the study area (Texas) during the storm. Previous studies show that snow accumulation is highly correlated with snow cover (Jonas et al., 2009). Thus, we chose to use the snow accumulation data from NOAA(https://www.nohrsc.noaa.gov/snowfall/), which provides complete coverage in the study area, to represent snow coverage. Fig. 6(b) shows the 72-hour snow accumulation measured at 12:00 AM on Feb 16. Compared with Fig. 6(a), we found that areas with increased NTL radiance (positive D) generally have higher snow accumulation. To eliminate the influence of outliers, we applied the bin-fitting method to quantify the relation between snow accumulation and NTL radiance change (Currit, 2002; Sanchez de Miguel et al., 2020). Specifically, we aggregate data points in the scatter plot into bins, each of which represents an interval of 0.5 inches snow accumulation (x-axis) and 0.1 NTL change ratio (y-axis). Then, we selected the bin with the highest point density in each interval in the x-axis (shown as orange dots in Fig. 7(a)) to derive a linear regression model. The positive coefficient of the regression ($\beta = 0.03$) indicates that the NTL difference ratio (D) is positively correlated with snowfall accumulation. This result confirms that snow coverage may enhance NTL radiance and justify the need for the snow effect adjustment.

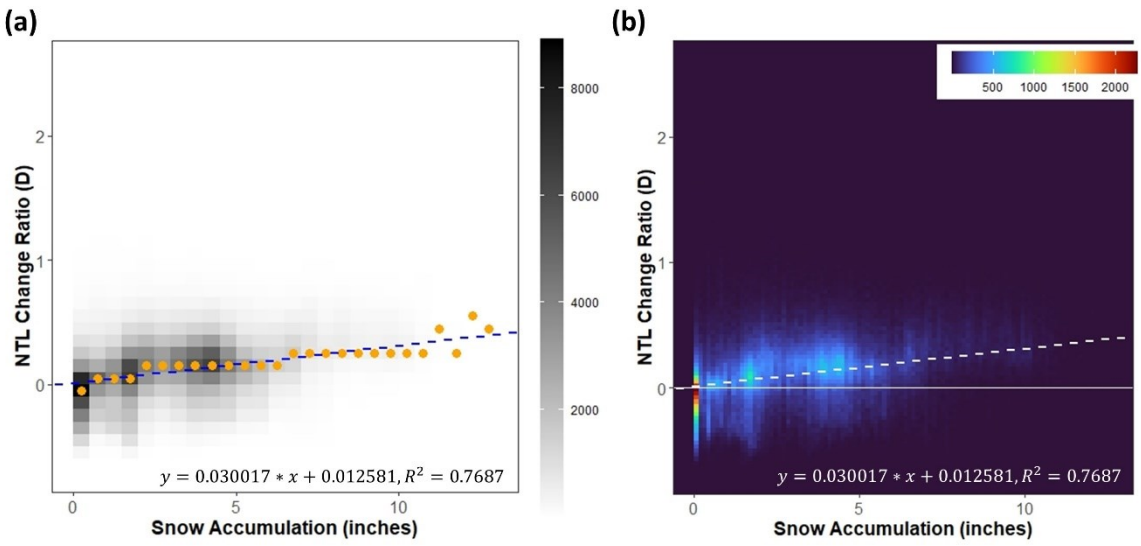

Fig. 7. (a) Bin-fit scatterplot between 72-hour snowfall and NTL difference ratio (D) of pixels in the Feb 16 NTL image. (b) Density plots between 72-hour snowfall and NTL difference ratio (D) of pixels in the Feb 16 NTL image, the white horizontal line (D = 0) represents no change.

The radiance adjustment includes the following steps. First, the adjustment models were developed in areas that did not experience extensive power outages (i.e., outage ratio < 10%, see Fig. 4(b)), assuming that the difference between the actual NTL radiance and simulated radiance was primarily caused by snow reflection. The outage ratio is the ratio of detected power outage time to total tracking time in the county, described in Section 2.2.3. The adjustment is expressed in Eq. 3, which is a linear equation of logarithmically transformed R_{actual} and $R_{simulated}$. We acknowledge that the correlation between R_{actual} and $R_{simulated}$ varies in different snow accumulation categories, and thus calculated the model parameters in seven snow accumulation categories (Table 3). In each category, we apply the bin-fitting method to derive a regression model between NTL radiance change (D) and snow accumulation. Details of models in each snow accumulation categories can be found in Fig. SI 2 to Fig. SI 8. Then, we use the derived

models to adjust the actual NTL radiance of pixels in different snow accumulation categories (Eq. 4).

$$\ln(R_{actual}) = f * \ln(R_{simulated}) + g \quad \text{Eq. 3}$$

$$R_{Adjusted} = e^{\frac{\ln(R_{actual}) - g}{f}} \quad \text{Eq. 4}$$

where e is the base of natural logarithms, f and g were calculated from pixels in each snow accumulation category.

Table 3. Coefficients in NTL radiance adjustment function by snow accumulation category

Snow accumulation (inches)	Slope (f)	Intercept (g)	Coefficients of determination (R^2)	Number of points
0 - 1	0.9464	1.0543	0.9671	36796
1 - 2	0.9707	0.7268	0.9483	50420
2 - 3	0.7815	1.4018	0.9681	36365
3 - 4	0.9780	1.2139	0.9738	43730
4 - 6	0.9278	1.3944	0.8896	67490
6 - 8	1.1255	0.7386	0.9849	20701
8 - 12	1.0645	0.9900	0.9867	10677

The actual radiance and adjusted radiance values were compared with simulated radiance using bin fit linear model in Fig. 8(a) & (c). The snow effect adjustment pulls the regression line (blue, where slope changed from 0.92589 to 0.99704 and intercept changed from 0.82176 to -0.27409) closer to the central line (black, where slope = 1 & intercept = 0), indicating a higher consistency between the adjusted radiance with the simulated radiance. The enhanced NTL values on Feb 16 that are potentially impacted by snow were adjusted and corrected to a normal level (based on the simulated NTL radiance on Feb 16). Comparing Fig. 8(a) with Fig. 8(c) and Fig. 8(b) with Fig. 8(d), we can see that the adjustment has alleviated the radiance biases caused by the snow effect.

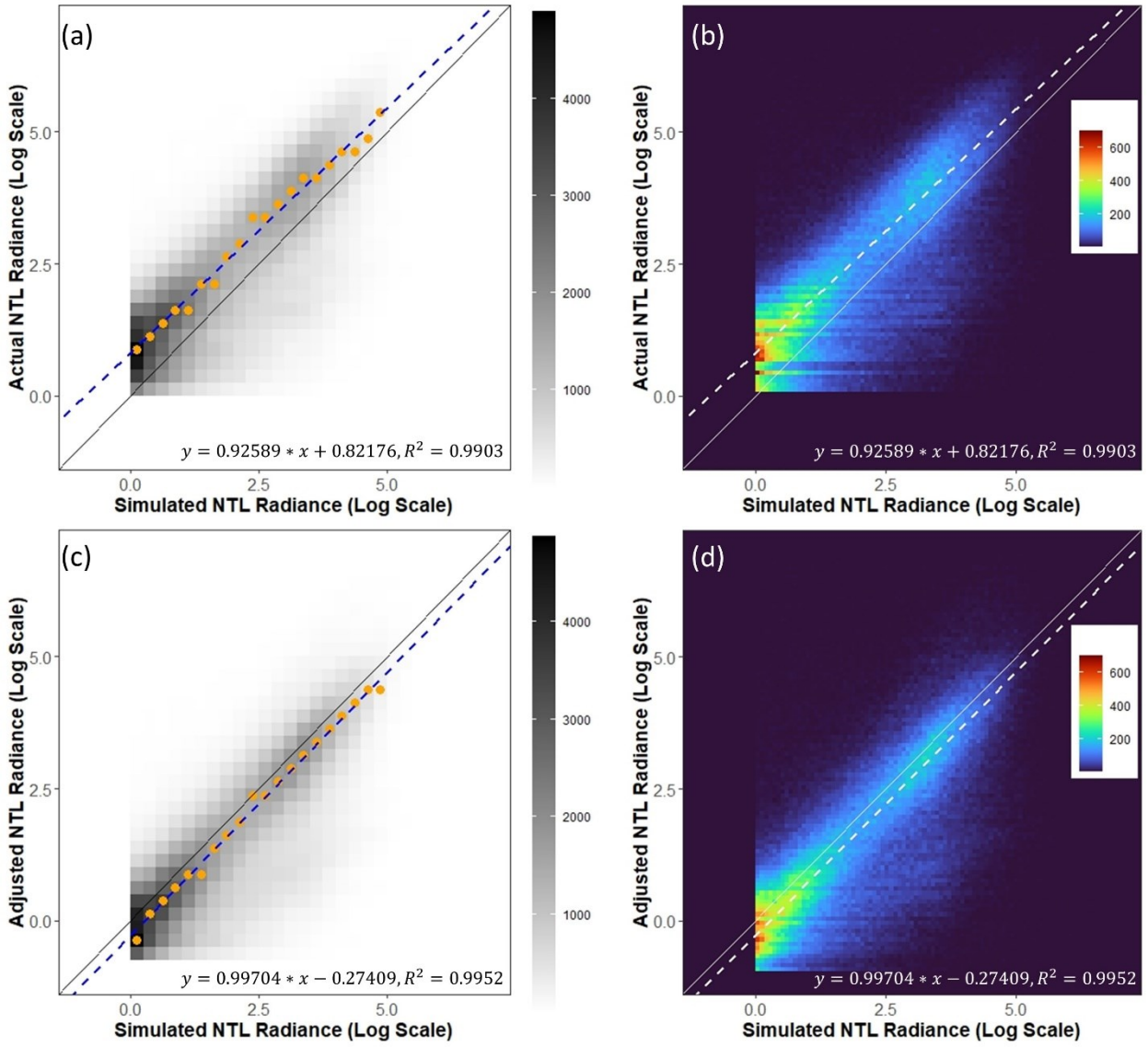

Fig. 8. (a) Bin-fit scatterplot between the actual NTL radiance and simulated NTL radiance on Feb 16 (bin width = 0.25 unit); (b) Density plots between the actual NTL radiance and simulated NTL radiance on Feb 16; (c) Bin-fit scatterplot between the actual NTL radiance and simulated NTL radiance on Feb 16 (bin width = 0.25 unit); (d) Density plots between the adjusted NTL radiance and simulated NTL radiance on Feb 16, black lines in (a)&(c) and white lines in (b)&(d) indicate the adjustment target (f(x) = x) and blue line indicates the actual bin fit to the target in all figures (equation and R^2 listed at the bottom of each graph)

4. Blackout Detection

Power outage is detected by comparing the adjusted NTL radiance on Feb 16 and the radiance in the normal condition (baseline radiance). The baseline radiance is a sample of radiance values on dates from Jan 1, 2020, to Jan 31, 2021, when the viewing angle and acquisition time is similar to that on Feb 16. We assume that blackout occurs in pixels where the radiance on Feb 16 reduces below a certain level (threshold) in comparison with the baseline radiance. The comparison was conducted only in high-quality pixels (Mandatory Quality Flag is 00) with similar viewing zenith angles (+/− 0.3°). Various thresholds are used in previous studies to detect power outages (Kar et al., 2021; Min et al., 2017; Shah et al., 2020). In this study, we tested three different thresholds to detect power outages using Eq. 5-7 respectively. The detected power outage by the three thresholds was validated against the county-level power outage tracking data. The threshold that generates the best correlation with the county-level power outage data was considered optimal and was used for the analysis in the next step. The parallel computing package (doSnow) in R developed by Analytics & Weston (2014) was applied to accelerate the pixel-wise computation.

$$R_{threshold1} = mean(R_{baseline}) - \beta_1 * \text{stdev}(R_{baseline}) \quad \text{Eq. 5}$$

$$R_{threshold2} = \beta_2 * mean(R_{baseline}) \quad \text{Eq. 6}$$

$$R_{threshold3} = min\,(R_{baseline}) \quad \text{Eq. 7}$$

where $R_{baseline}$ is the radiance values from Jan 1, 2020, to Jan 31, 2021 when the viewing angle is similar to that on Feb 16, 2021. These radiance values are considered the baseline that represents radiance values at the normal time. As an example, the red bounding

boxes in Fig. 5 highlight the baseline radiance values in the four pixels. $R_{threshold1-3}$ are the thresholds below which power outages are determined. $Stdev$, $mean$, and min are functions to calculate standard deviation, mean, and minimum from the baseline radiance values.

Using the three thresholds, pixels in the Feb 16 images are classified into outage pixels (radiance < threshold) and non-outage pixels (radiance ≥ threshold). The ratio of power outages is calculated as the division of outage pixels by total pixels in counties and census tracts. Instead of using arbitrary values, the coefficient β_1 and β_2 in $R_{threshold1}$ and $R_{threshold2}$ are derived from an iterative program. The program uses all possible values of β_1 in [0,1] and $\beta_2$in [0,2] with an increment of 0.01 to calculate power outage ratios in counties and conducts regression analysis between the power outage ratios detected from NTL and the outage ratios calculated from the outage tracking data. The optimal values of β_1 and β_2 are selected when the coefficient of determination (R^2) of the regression analysis is the highest, indicating the highest consistency between the two datasets. Fig. 9 shows the changing pattern of R^2 with increasing values of β_1 and β_2 in the iterative program. The values of β_1 and β_2 at the peaks of the curves are considered optimal and applied in Eq. 5&6 to calculate $R_{threshold1}$ and $R_{threshold2}$ respectively. The higher R^2 in the blue line shows that adjusted radiance achieved a higher consistency with the outage tracking data than the original radiance.

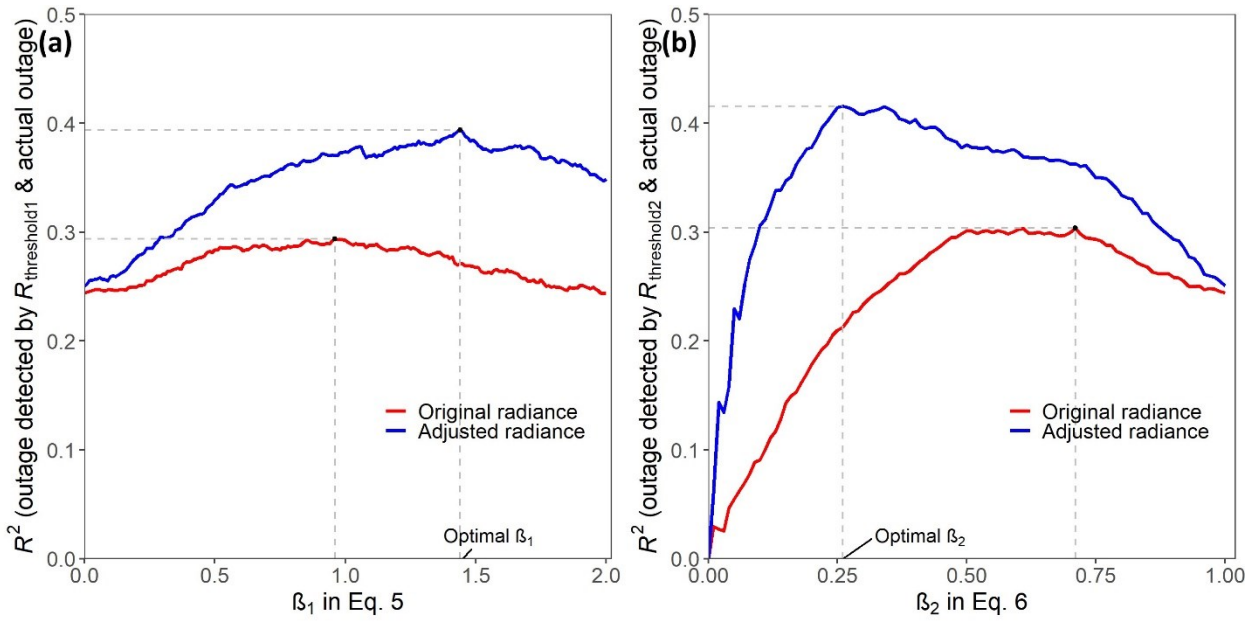

Fig. 9. Changes of R^2 with increasing β_1 (left) and β_2 (right) in the iterative program. Blue and red curves are calculated with adjusted and original radiance respectively.

To evaluate the effect of the adjustment in Section 3, changing patterns of R^2 calculated from the original NTL images (red lines) and adjusted NTL images (blue lines) are illustrated in Table 4, indicating that the adjustment process has improved the ability of the NTL images for power outage detection. Regression analysis was used to validate the power outage ratios calculated from NTL images against the ratios calculated from outage tracking data at the county level. A higher coefficient of determination (R^2) implies a better match of power outages detected in the two data sources. Comparing the three thresholds, the power outage ratio calculated using $R_{threshold2}$ (Eq. 6) has the highest correlation (R^2 = 0.4157) with the ratios from the outage tracking data, followed by the ratios calculated by $R_{threshold1}$ (Eq. 5) & $R_{threshold3}$ (Eq. 7). Thus, the power outage pixels and ratios of the outage pixels calculated with $R_{threshold2}$ (Eq. 6) are used in the following analysis.

Table 4. Highest coefficient of determination (R^2) in each NTL threshold and the optimal coefficient β (if applicable) that generates the highest R^2.

	$R_{threshold1}$ (Eq. 5)	$R_{threshold2}$ (Eq. 6)	$R_{threshold3}$ (Eq. 7)
Original NTL radiance	0.2938 (β_1 = 0.96)	0.3035 (β_2 = 0.71)	0.2882
Adjusted NTL radiance	0.3939 (β_1 = 1.44)	0.4157 (β_2 = 0.26)	0.3827

The outage pixels derived from the threshold with the best performance ($R_{threshold2}$) were visualized in Fig. 10 (a). A zoom-in view for three metropolitan areas, Houston, Dallas-Fort Worth, and Austin-San Antonio, was shown in Fig. 10(b)–(d). The outage occurred around suburban areas or the edges of the urban areas in Dallas, Austin, and San Antonio, whereas large areas in the center of Houston suffered from blackouts. At the pixel level (Fig. 10(c)), areas surrounding Houston were heavily impacted by the outage. The western area of Texas did not experience widespread outages.

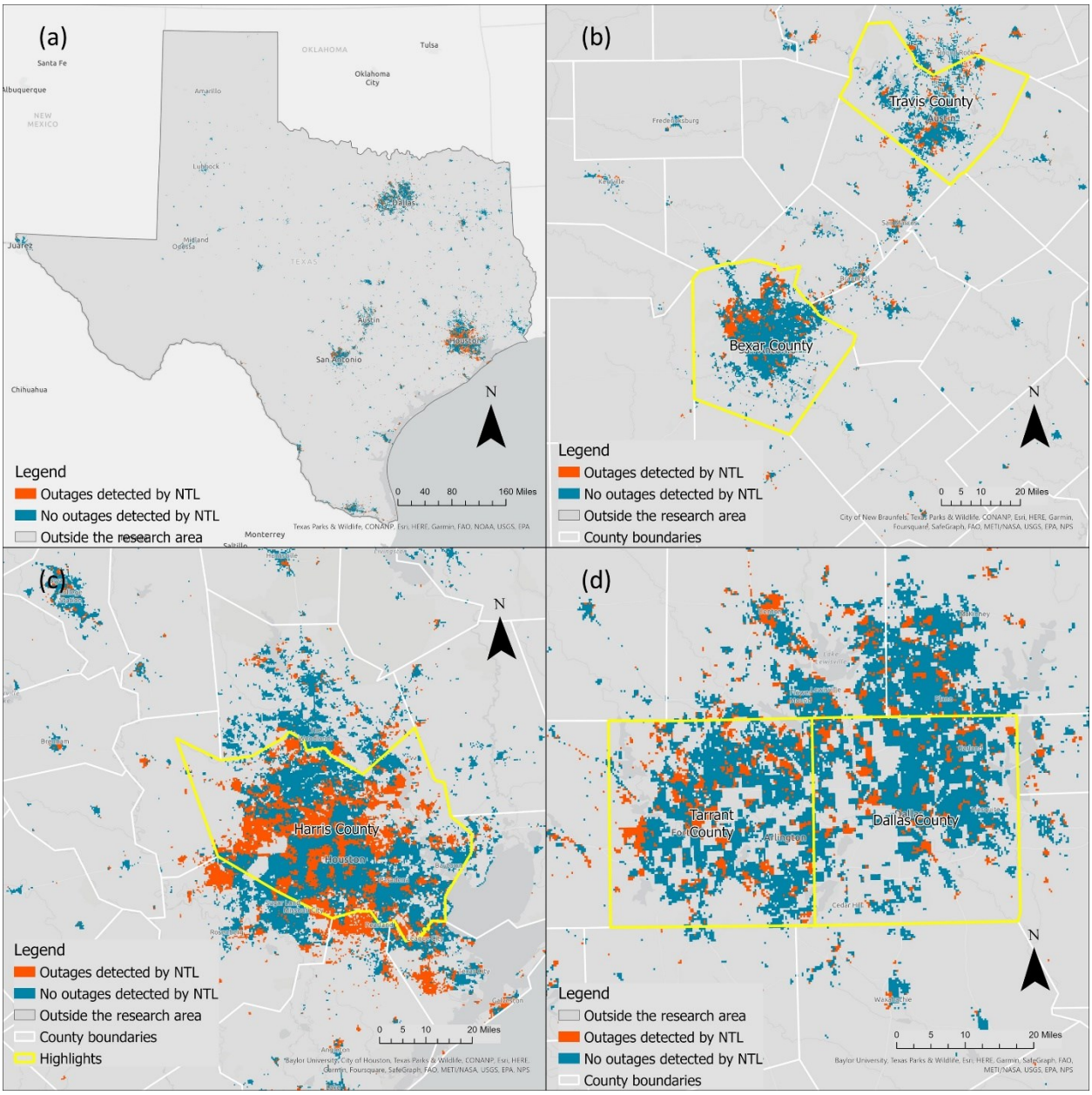

Fig. 10. a) Outage pixels from NTL images in the declared disaster counties in Texas, b) Zoom-in view of Austin (Travis County) and San Antonio (Bexar County), c) zoom-in view of Houston (Harris County), d) zoom-in view of Dallas (Dallas County) and Fort Worth (Tarrant County).

Fig. 11(a)&(b) show outage ratios in counties and each census tract, where coastal counties near the Gulf of Mexico experienced large outage ratios. The patterns of NTL power outage ratios generally agree with the outage ratios calculated in Fig. 4(b). However, within

Harris County, the outage tracking data show a low outage ratio (Fig. 4(b)) whereas the outage ratio detected from NTL (Fig. 11(a)) shows the opposite. Considering the large industrial areas in Houston and differences in electricity consumption between residential clients and industrial clients, the power outage tracking data in residential areas can be diluted by the large regularly supplied industrial electricity consumption. Overall, regardless of a few places that show discrepancies between outage tracking data and NTL outage ratio, the spatial patterns of county-level power outage ratios derived from the two datasets are similar, plus the NTL images can provide timely power outage detection at a higher resolution (~500m).

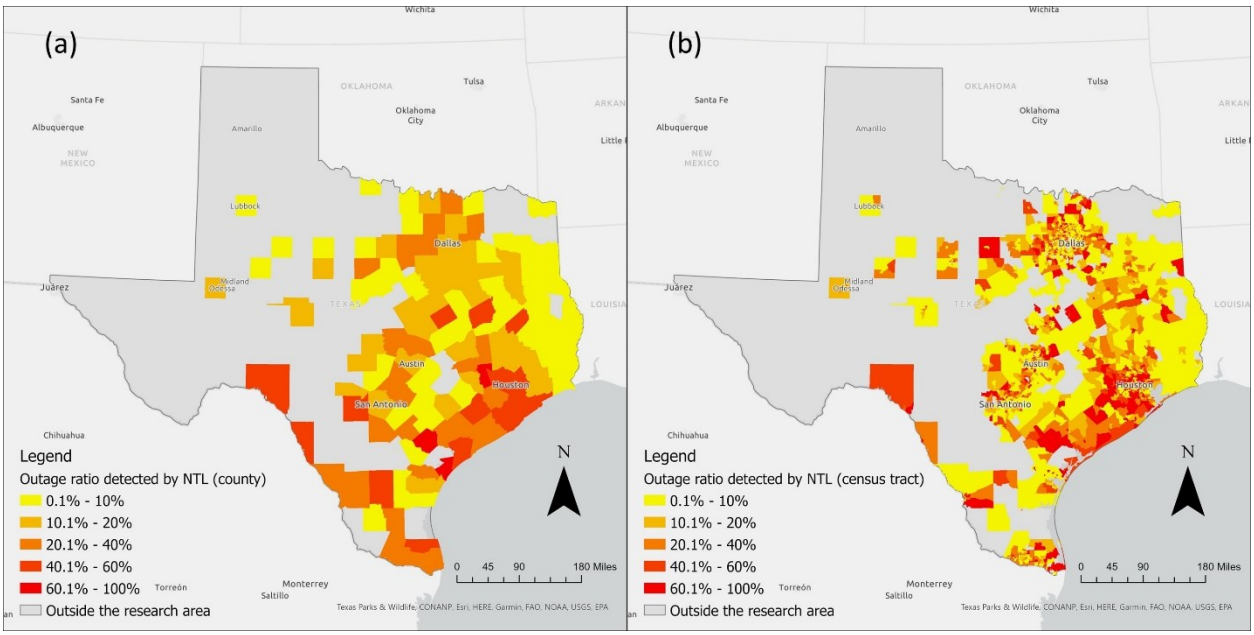

Fig. 11. a) Power outage ratios aggregated in counties, b) Power outage ratios aggregated in census tracts.

5. Correlation Analysis

Pearson correlation analyses were then used to analyze the relations between outage ratios detected in NTL images and socio-economic variables listed in Table 2 at both the county level

and the census tract level. Table 5 lists the *p* values and Pearson correlation coefficients between the power outage ratio and each socio-economic variable. Socio-economic variables that have significant correlations (*p*-value < 0.05) with power outage ratios are highlighted in bold font. At the county level, the blackouts tend to occur in Hispanic/Latino communities and communities with newer buildings. At the census tract level, power outages are more likely to happen in Latino/Hispanic communities, communities with fewer white populations, a longer commuting time, lower unemployment ratios, and higher median housing value. The results show that the relations between disadvantaged population groups and power outages vary at the two spatial scales, except that Ratios of the Hispanic/Latino population show strong correlations at both scales.

Table 5. The statistics (*p*-value and Pearson correlation coefficient) of the correlation models between socio-economic variables and the NTL power outage ratio

Population group	NTL outage (county)			NTL outage (census tract)		
	p-value	Pearson's *r*	Degree of freedom	*p*-value	Pearson's *r*	Degree of freedom
Ratio of White only	0.764	0.027	123	**0.013***	**-0.038**	4180
Ratio of African American only	0.184	-0.120	123	0.194	0.020	4180
Ratio of American Indian and Alaska Native alone	0.097	-0.149	123	0.135	-0.023	4180
Ratio of Asian	0.097	0.149	123	0.139	0.023	4180
Ratio of Latino/Hispanic	**0.000*****	**0.334**	123	**0.000*****	**0.083**	4180
Ratio of 25 years old + and hold a degree less than college degree	0.356	-0.083	123	0.546	0.009	4180
Ratio of Commute time less than 30 minutes	0.109	-0.144	123	**0.000*****	**-0.171**	4180
Ratio of income lower than poverty level	0.484	0.063	123	0.360	-0.014	4180
Median household income	0.331	0.088	123	0.266	0.017	4180
Unemployment ratio	0.281	-0.097	123	**0.000*****	**-0.069**	4180
Renter-occupied housing ratio	0.889	0.013	123	0.120	-0.024	4180
Ratio of constructions built after 2000	**0.022***	**0.205**	123	0.559	-0.009	4180
Median value	0.266	0.100	123	**0.018***	**0.037**	4180

Median gross rent	0.299	0.094	123	0.803	0.004	4180

*** $p<0.001$, ** $p<0.01$, * $p<0.05$

6. Discussion

This study presents an analytical workflow to detect power outages from daily Black Marble NTL images and the application of this approach in 2021 Winter Storm Uri. Compared to other data sources (e.g., the county-level power outage tracking data), the NTL-based approach can detect power outages at a finer spatial resolution (~500m), providing important support for emergency response and assessment of infrastructure damage and recovery. Through exploratory data analysis, we discovered the effects of the viewing angle and ground snow reflection on the NTL radiance, which prohibits a direct comparison between the images captured in the storm with the images in normal times (baseline condition). Additionally, the snow and angular effects show strong spatial variation, and thus cannot be corrected using a global model. To this end, we developed radiance adjustment models to reduce the biases introduced by various viewing angles and snow reflection over the study area. The model training at each pixel creates a substantial computational load, which was effectively addressed by parallel algorithms. In the validation against the outage tracking data, the adjusted NTL radiance shows an improved ability in power outage detection than the non-adjusted images.

The power outage detection was conducted by comparing the adjusted NTL radiance on Feb 16 with the radiance in the normal condition (baseline). Due to the instability of NTL radiance, choosing images on a specific date as the baseline may introduce uncertainties caused by radiance fluctuations on that day. Instead, we used a sample of dates in 2020 and 2021 when the viewing angle was similar to that on Feb 16 to represent the baseline radiance. Another challenge we faced in this study is choosing an appropriate threshold to detect power outages.

The choice of the threshold determines the extent of radiance reduction that should be classified as power outages. Various thresholds are used in previous studies, which are somehow arbitrary and lack empirical validation. To address this issue, we developed an iterative algorithm to search for the optimal threshold that can generate the highest correlation between the outage detected from NTL and the outage tracking data. This approach fuses the outage tracking data and NTL images to find the threshold to obtain a finer-resolution (~500m) power outage detection.

With the developed power outage detection approach, the second objective is to evaluate environmental justice issues in Winter Storm Uri. Our hypothesis is that disadvantaged populations are disproportionally exposed to power outages in the storm. The resultant power outage map at a finer resolution (~500m) enables the evaluation of the hypothesis at the census tract level. The statistical analyses show that the ratio of the Latino/Hispanic population has a significant correlation with power outage ratios at both the county and census-tract level. This result confirms the finding in the previous studies by Lee et al. (2021) and Flores et al. (2022). As Texas is the state with the second largest Hispanic population (Nielsen-Gammon, 2011), this result signals an alarming trend that the Hispanic population may be disproportionally exposed to vulnerable electric power systems in natural disasters. Despite the statistical significance, the correlations between power outages and other disadvantaged population groups are not very strong (relatively low Pearson's *r* values). This result is possibly due to the limited data sample in one specific event. To fully understand the environmental justice issues, further research with improved outage detection techniques should be conducted in more and other hazard events to confirm the findings from this study.

The proposed method can be improved in the following aspects. First, the NTL should be further decomposed into different types of human activities. The captured NTL radiance can be generated from road traffic, industrial sites (e.g., oil refineries), and critical facilities that have an emergency power supply (e.g., hospitals). The illumination from these facilities may influence the detection of power outages that hit residential households. A future improvement is to classify the NTL radiance into different land use and land cover types, from which the power outage occurred in residential areas can be differentiated. The differentiated power outage detection will provide more reliable data to study environmental justice issues in the storm. Second, the NTL radiance captured in the Black Marble images is highly dependent on weather conditions. The introduced approach requires a clear sky to detect changes in NTL radiance, which may not occur in some disaster events. In this study, Feb 16 is the only date during the storm when there are sufficient high-quality pixels (clear sky) to observe NTL in the study area. On other dates, most urban areas are fully or partially covered by clouds, preventing the observation of NTL on the ground. Additionally, the NTL variation is affected by complex factors other than snow cover, which lead to only a moderate fit between outage tracking data and outages detected by NTL. Such factors can include but are not limited to the ground condition (e.g., snow cover, flood inundation) and atmospheric conditions (e.g., moisture). In future research, we would further improve the method to reduce biases and uncertainties introduced by these factors.

7. Conclusion

This study utilizes NASA's daily Black Marble images to detect power outages in Winter Storm Uri that hit Texas in 2021. The study introduces a complete workflow from image selection, processing, and radiance adjustment to power outage detection. The analysis uncovers the effects

of viewing angle and snow cover on NTL radiance and introduces adjustment methods to mitigate the effects. The validation against an additional data source (the outage tracking data) indicates an improved NTL quality after the adjustment. The derived power outage maps at a finer resolution (~500m) provide important support for emergency response, disaster relief, and recovery. Using publicly available data sources, the developed methodology is widely applicable to other hazardous events in other regions, which provide important support for enhancing community and infrastructure resilience. Furthermore, we analyzed the relations between the ratios of detected power outages and ratios of several disadvantaged population groups, aiming to discover environmental injustice and social disparities in this disaster. The results show that the Hispanic/Latino population tends to reside in communities that are impacted by power outages, which echoes findings in peer studies about this storm. This finding raises concerns about potential environmental justice issues in natural disasters, which deserve further investigation with improved data and techniques.

Data Availability Statement

The data is freely available upon request.

Conflicts of Interest

The authors declare no conflict of interest.

References

Alexander, M., & Sara, H. (2017, December 6). *Nearly half of all U.S. electricity customers have smart meters*. https://www.eia.gov/todayinenergy/detail.php?id=34012

Analytics, R., & Weston, S. (2014). doSNOW: Foreach parallel adaptor for the snow package. *R Package Version*, *1*(14), 12.

Azad, S., & Ghandehari, M. (2021). A study on the association of socioeconomic and physical cofactors contributing to power restoration after hurricane Maria. *IEEE Access*, *9*, 98654–98664.

Boroojeni, K. G., Amini, M. H., & Iyengar, S. S. (2017). *Smart grids: Security and privacy issues*. Springer.

Casey, J. A., Fukurai, M., Hernández, D., Balsari, S., & Kiang, M. V. (2020). Power outages and community health: A narrative review. *Current Environmental Health Reports*, *7*(4), 371–383.

Chang, S. E. (2003). Evaluating disaster mitigations: Methodology for urban infrastructure systems. *Natural Hazards Review*, *4*(4), 186–196.

Cole, T. A., Wanik, D. W., Molthan, A. L., Román, M. O., & Griffin, R. E. (2017). Synergistic use of nighttime satellite data, electric utility infrastructure, and ambient population to improve power outage detections in urban areas. *Remote Sensing*, *9*(3), 286.

Currit, N. (2002). Inductive regression: Overcoming OLS limitations with the general regression neural network. *Computers, Environment and Urban Systems*, *26*(4), 335–353. https://doi.org/10.1016/S0198-9715(01)00045-X

Cutter, S. L., Boruff, B. J., & Shirley, W. L. (2003). Social Vulnerability to Environmental Hazards*. *Social Science Quarterly*, *84*(2), 242–261. https://doi.org/10.1111/1540-6237.8402002

Deshmukh, A., Oh, E. H., & Hastak, M. (2011). Impact of flood damaged critical infrastructure on communities and industries. *Built Environment Project and Asset Management*.

Dewitz, J., & U.S. Geological Survey. (2021). *National Land Cover Database (NLCD) 2019 Products (ver. 2.0, June 2021)—ScienceBase-Catalog*. https://www.sciencebase.gov/catalog/item/5f21cef582cef313ed940043

Dominianni, C., Ahmed, M., Johnson, S., Blum, M., Ito, K., & Lane, K. (2018). Power outage preparedness and concern among vulnerable New York City residents. *Journal of Urban Health*, *95*(5), 716–726.

Federal Agency Management Agency. (2021a). *President Joseph R. Biden, Jr. Approves Major Disaster Declaration for Texas | FEMA.gov*. https://www.fema.gov/press-release/20210220/president-joseph-r-biden-jr-approves-major-disaster-declaration-texas

Federal Agency Management Agency. (2021b). *Texas Winter Storm Survivors in 18 Additional Counties Can Apply for Federal Disaster Assistance | FEMA.gov*. https://www.fema.gov/press-release/20210227/texas-winter-storm-survivors-18-additional-counties-can-apply-federal

Federal Agency Management Agency. (2021c). *Texas Winter Storm Survivors in 31 Additional Counties Can Apply for Federal Disaster Assistance*. https://www.fema.gov/press-release/20210222/texas-winter-storm-survivors-31-additional-counties-can-apply-federal

Flores, N. M., McBrien, H., Do, V., Kiang, M. V., Schlegelmilch, J., & Casey, J. A. (2022). The 2021 Texas Power Crisis: Distribution, duration, and disparities. *Journal of Exposure Science & Environmental Epidemiology*, 1–11. https://doi.org/10.1038/s41370-022-00462-5

Goodchild, M. F. (2007). Citizens as sensors: The world of volunteered geography. *GeoJournal*, *69*(4), 211–221. https://doi.org/10.1007/s10708-007-9111-y

Guan, X., & Chen, C. (2014). Using social media data to understand and assess disasters. *Natural Hazards*, *74*, 837–850.

Hendricks, M. D., & Van Zandt, S. (2021). Unequal protection revisited: Planning for environmental justice, hazard vulnerability, and critical infrastructure in communities of color. *Environmental Justice*, *14*(2), 87–97.

Homer, C., Dewitz, J., Jin, S., Xian, G., Costello, C., Danielson, P., Gass, L., Funk, M., Wickham, J., Stehman, S., Auch, R., & Riitters, K. (2020). Conterminous United States land cover change patterns 2001–2016 from the 2016 National Land Cover Database. *ISPRS Journal of Photogrammetry and Remote Sensing*, *162*, 184–199. https://doi.org/10.1016/j.isprsjprs.2020.02.019

Ivanova, I. (2021, February 25). *Texas winter storm costs could top $200 billion—More than hurricanes Harvey and Ike*. https://www.cbsnews.com/news/texas-winter-storm-uri-costs/

Jin, S., Homer, C., Yang, L., Danielson, P., Dewitz, J., Li, C., Zhu, Z., Xian, G., & Howard, D. (2019). Overall Methodology Design for the United States National Land Cover Database 2016 Products. *Remote Sensing*, *11*(24), Article 24. https://doi.org/10.3390/rs11242971

Jonas, T., Marty, C., & Magnusson, J. (2009). Estimating the snow water equivalent from snow depth measurements in the Swiss Alps. *Journal of Hydrology*, *378*(1), 161–167. https://doi.org/10.1016/j.jhydrol.2009.09.021

Kar, B., Bobeck, J., Moss, T., & Hughes, D. (2021). Spatiotemporal Tracking of Wide Area Power Outage from Night-Time Light Imagery. *2021 IEEE International Geoscience and Remote Sensing Symposium IGARSS*, 566–569.

Klinger, C., Landeg, O., & Murray, V. (2014). Power outages, extreme events and health: A systematic review of the literature from 2011-2012. *PLoS Currents*, *6*.

Kwasinski, A., Andrade, F., Castro-Sitiriche, M. J., & O'Neill-Carrillo, E. (2019). Hurricane maria effects on puerto rico electric power infrastructure. *IEEE Power and Energy Technology Systems Journal*, *6*(1), 85–94.

Lam, N. S. N., Reams, M., Li, K., Li, C., & Mata, L. P. (2016). Measuring Community Resilience to Coastal Hazards along the Northern Gulf of Mexico. *Natural Hazards Review*, *17*(1), 04015013. https://doi.org/10.1061/(ASCE)NH.1527-6996.0000193

Lee, C.-C., Maron, M., & Mostafavi, A. (2021). *Community-scale Big Data Reveals Disparate Impacts of the Texas Winter Storm of 2021 and its Managed Power Outage* (arXiv:2108.06046). arXiv. https://doi.org/10.48550/arXiv.2108.06046

Levin, N., & Zhang, Q. (2017). A global analysis of factors controlling VIIRS nighttime light levels from densely populated areas. *Remote Sensing of Environment*, *190*, 366–382. https://doi.org/10.1016/j.rse.2017.01.006

Li, L., Ma, Z., & Cao, T. (2020). Leveraging social media data to study the community resilience of New York City to 2019 power outage. *International Journal of Disaster Risk Reduction*, *51*, 101776.

Li, X., Ma, R., Zhang, Q., Li, D., Liu, S., He, T., & Zhao, L. (2019). Anisotropic characteristic of artificial light at night – Systematic investigation with VIIRS DNB multi-temporal

observations. *Remote Sensing of Environment*, *233*, 111357. https://doi.org/10.1016/j.rse.2019.111357

Mao, H., Thakur, G., Sparks, K., Sanyal, J., & Bhaduri, B. (2018). Mapping near-real-time power outages from social media. *International Journal of Digital Earth*.

Mastroianni, E., Lancaster, J., Korkmann, B., Opdyke, A., & Beitelmal, W. (2021). Mitigating infrastructure disaster losses through asset management practices in the Middle East and North Africa region. *International Journal of Disaster Risk Reduction*, *53*, 102011.

Min, B. K., O'Keeffe, Z., & Zhang, F. (2017). Whose power gets cut? Using high-frequency satellite images to measure power supply irregularity. *Using High-Frequency Satellite Images to Measure Power Supply Irregularity (June 29, 2017). World Bank Policy Research Working Paper*, *8131*.

Nielsen-Gammon, J. W. (2011). The changing climate of Texas. *The Impact of Global Warming on Texas*, *39*, 86.

Public Utility Commission of Texas. (2022). *Alphabetical Directory of Retail Electric Providers*. https://www.puc.texas.gov/industry/electric/directories/rep/alpha_rep.aspx

Qiang, Y., Huang, Q., & Xu, J. (2020). Observing community resilience from space: Using nighttime lights to model economic disturbance and recovery pattern in natural disaster. *Sustainable Cities and Society*, *57*, 102115.

Ribeiro, F. N., Benevenuto, F., & Zagheni, E. (2020). How biased is the population of Facebook users? Comparing the demographics of Facebook users with census data to generate correction factors. *12th ACM Conference on Web Science*, 325–334.

Ribeiro, F. N., Henrique, L., Benevenuto, F., Chakraborty, A., Kulshrestha, J., Babaei, M., & Gummadi, K. P. (2018). Media bias monitor: Quantifying biases of social media news outlets at large-scale. *Twelfth International AAAI Conference on Web and Social Media*.

Rice, D., & Aspegren, E. (2021). *At least 4 dead, 150M people under winter advisories as "unprecedented" storm stretches across 25 states; 4.3M without power in Texas*. USA TODAY. https://www.usatoday.com/story/news/nation/2021/02/15/winter-storm-texas-power-outages-south-ice-snow/4487366001/

Román, M. O., Stokes, E. C., Shrestha, R., Wang, Z., Schultz, L., Carlo, E. A. S., Sun, Q., Bell, J., Molthan, A., & Kalb, V. (2019). Satellite-based assessment of electricity restoration efforts in Puerto Rico after Hurricane Maria. *PloS One*, *14*(6), e0218883. https://doi.org/10/ghmm7j

Román, M. O., Wang, Z., Shrestha, R., Yao, T., & Kalb, V. (2019). Black marble user guide version 1.0. *NASA: Washington, DC, USA*.

Román, M. O., Wang, Z., Sun, Q., Kalb, V., Miller, S. D., Molthan, A., Schultz, L., Bell, J., Stokes, E. C., Pandey, B., Seto, K. C., Hall, D., Oda, T., Wolfe, R. E., Lin, G., Golpayegani, N., Devadiga, S., Davidson, C., Sarkar, S., … Masuoka, E. J. (2018). NASA's Black Marble nighttime lights product suite. *Remote Sensing of Environment*, *210*, 113–143. https://doi.org/10.1016/j.rse.2018.03.017

Sanchez de Miguel, A., Kyba, C. C., Zamorano, J., Gallego, J., & Gaston, K. J. (2020). The nature of the diffuse light near cities detected in nighttime satellite imagery. *Scientific Reports*, *10*(1), 7829.

Shah, Z., Hsu, F.-C., Elvidge, C. D., & Taneja, J. (2020). Mapping Disasters & Tracking Recovery in Conflict Zones Using Nighttime Lights. *2020 IEEE Global Humanitarian Technology Conference (GHTC)*, 1–8.

Sun, H., Wang, Z., Wang, J., Huang, Z., Carrington, N., & Liao, J. (2016). Data-driven power outage detection by social sensors. *IEEE Transactions on Smart Grid*, *7*(5), 2516–2524.

Tan, X., Zhu, X., Chen, J., & Chen, R. (2022). Modeling the direction and magnitude of angular effects in nighttime light remote sensing. *Remote Sensing of Environment*, *269*, 112834. https://doi.org/10.1016/j.rse.2021.112834

Tweed, K. (2016, October 14). *Texas Has Millions of Smart Meters. So Why Haven't Third-Party Energy Services Blossomed?* https://www.greentechmedia.com/articles/read/texas-highlights-the-challenge-of-one-click-energy-services

Upton, G., & Cook, I. (1996). *Understanding statistics*. Oxford University Press.

Wang, Z., Román, M. O., Kalb, V. L., Miller, S. D., Zhang, J., & Shrestha, R. M. (2021). Quantifying uncertainties in nighttime light retrievals from Suomi-NPP and NOAA-20 VIIRS Day/Night Band data. *Remote Sensing of Environment*, *263*, 112557. https://doi.org/10.1016/j.rse.2021.112557

Wang, Z., Román, M. O., Sun, Q., Molthan, A. L., Schultz, L. A., & Kalb, V. L. (2018). Monitoring disaster-related power outages using NASA black marble nighttime light product. *ISPRS Int. Arch. Photogramm. Remote Sens. Spat. Inf. Sci*, 1853–1856.

Wickham, J., Stehman, S. V., Sorenson, D. G., Gass, L., & Dewitz, J. A. (2021). Thematic accuracy assessment of the NLCD 2016 land cover for the conterminous United States. *Remote Sensing of Environment*, *257*, 112357. https://doi.org/10.1016/j.rse.2021.112357

Xu, J., & Qiang, Y. (2021). Spatial assessment of community resilience from 2012 Hurricane Sandy using nighttime light. *Remote Sensing*, *13*(20), 4128.

Yang, L., Jin, S., Danielson, P., Homer, C., Gass, L., Bender, S. M., Case, A., Costello, C., Dewitz, J., & Fry, J. (2018). A new generation of the United States National Land Cover Database: Requirements, research priorities, design, and implementation strategies. *ISPRS Journal of Photogrammetry and Remote Sensing*, *146*, 108–123.

Zhao, X., Yu, B., Liu, Y., Yao, S., Lian, T., Chen, L., Yang, C., Chen, Z., & Wu, J. (2018). NPP-VIIRS DNB daily data in natural disaster assessment: Evidence from selected case studies. *Remote Sensing*, *10*(10), 1526. https://doi.org/10/ghmkg3